Journal of Nuclear Materials 544 (2021) 152699

Contents lists available at ScienceDirect

Journal of Nuclear Materials

journal homepage: www.elsevier.com/locate/jnucmat

A NMR and SANS study of alkali-borosilicate behaviour under thermal neutron irradiation

R. Boffy[a,*], L. Martel[b], R. Schweins[a], J. Somers[b], J. Beaucour[a], F.J. Bermejo[c]

[a] Institut Laue-Langevin, 71 avenue des Martyrs, CS 20156, 38042 Grenoble Cedex 9, France
[b] European Commission, Joint Research Centre, Institute for Transuranium Elements, P.O. Box 2340, D-76125 Karlsruhe, Germany
[c] Instituto de Estructura de la Materia, Consejo Superior de Investigaciones Cientificas, Serrano 123, E-20886 Madrid, Spain

ARTICLE INFO

Article history:
Received 9 April 2020
Revised 15 November 2020
Accepted 22 November 2020
Available online 5 December 2020

PACS:
61.80.Hg
81.05.Kf
61.82.Ms
29.25.Dz
28.20.Fc

Keywords:
Borosilicate Glass
Irradiation Damage
Neutron Scattering
NMR Characterization
Thermal Neutron Irradiation

ABSTRACT

The internal structure of several alkali-borosilicate glasses has been studied when exposed to a high thermal neutron flux. More specifically, the different glasses we are interested in are widely used around the globe for neutron guide manufacturing and show drastically different resistance to irradiation. Samples were irradiated with the thermal flux from T4 experimental tube in ILL's High Flux Reactor up to a fluence of several 10^{17} n/cm^2. The experimental tools employed for the structural analysis were Nuclear Magnetic Resonance (NMR) and Small Angle Neutron Scattering (SANS). NMR measurements allowed to detect the modification of atoms' close environment and these results have been correlated to evolutions at macroscopic scale. In addition, neutron scattering measurements have demonstrated the possibility to detect phase segregation in a zinc-alkali-borosilicate.

1. Introduction

Borosilicate glasses are employed for the manufacturing of the vast majority of neutron guides. These equipments, once evacuated, connect an intense source to scattering experiments. Their use spread across the globe because they allowed to increase the number of instruments per source by two or three for a negligible cost compared to building a new source. The development of super-mirror technology has increased the flux transported in these guides and, proportionally, accelerated the ageing phenomena [1,2]. The need of present study comes from the unexpected failures of neutron guides in different scientific institutes [3–5]. The origin of these incidents was found to be $^{10}B(n,\alpha)^7Li$ reactions that modify the vitreous structure and have consequences at the macroscopic scale, such as changes in density. The use of borated substrate is mandatory to provide a thermal neutron shield to the environment. The reasons behind the studies carried on neutron guide glasses is to understand the reasons behind glass irradiation induced breaking and suggest best candidates for future glass guide manufacturing. These suggestions could me made in terms of industrial products as well as compositions rules.

On a larger scale, borosilicate glasses are used for high-level nuclear waste conditioning [6–8]. To forecast the stability of these waste container throughout time, there behaviour was studied under various types of irradiation such as electrons [9–13], neutrons [14,15], helium ions [12,16], xenon ions [17,18], Silver ions [19], gold ions [20], etc. Yang *et al.* [12] compared the effects of helium ions and electrons on a borosilicate glass. They showed that electrons were increasing the network polymerization by reducing the amount of Q_2 silicon tetrahedra and increasing Q_3 and Q_4, whereas He ions were not noticeably affecting these parameters. They explained the results as if the ballistic mixing created by He stopping counterbalanced the effects of electronic slowing down. On the contrary, He ions were more efficient than the electrons in modifying the material hardness. Peuget *et al.* [21] studied the structural effects of radiation on a ternary sodium borosilicate glass by means of neutron and ion beams. They showed that ion irradiation had similar consequences on the glass network than fast quenching (above 3×10^4 K/min). As far as the boron coordination

* Corresponding author.
E-mail address: romain.boffy@cea.fr (R. Boffy).

https://doi.org/10.1016/j.jnucmat.2020.152699
0022-3115/

characteristics are concerned, the study show that xenon ion irradiation was converting BO_4^- into BO_3 units.

Studied glasses have shown remarkable differences in term of macroscopic behaviour. When used as neutron mirror substrate, Borofloat and N-ZK7 are known to splinter when they reach a grazing angle fluence around 2.0×10^{15} n/cm^2 and 2.8×10^{16} n/cm^2, respectively. On the opposite N-BK7 and S-BSL7 were already brought above a grazing fluence of 1.5×10^{17} n/cm^2 without any sign of rupture [22]. Boroloaf, N-ZK7 and N-BK7 glasses are worldwidely used for neutron guide manufacturing for many years, while S-BSL7 is a possible candidate for future guide manufacturing.

In terms of bulk properties, Borofloat and N-ZK7 shrink under irradiation up to 2 % and 1 %, respectively. This trend has been correlated to a compaction of their silica network which is unstable under irradiation and compacts up to 3 % [23]. In the case of a grazing angle irradiation, this leads to the creation of stresses that may end up with their release by brittle rupture of the material. These stresses were highlighted thanks to grazing angle irradiation of thin glass plates that deformed [24]. On the contrary, N-BK7 and S-BSL7 are more stable and have a very similar behaviour. They swell under irradiation but at a rate which is, on the absolute, 10 and 5 times smaller that Borofloat and N-ZK7, respectively. This was correlated to their homogeneous internal structure that consists mainly in a combination of boron and silicon atoms that are known to form reedmergnerite like structures. In these glasses, the silicon rich phase is replaced by these mixed borosilicate groups that are more stable under irradiation than a pure silica network [20,25,26].

In a previous paper [27], the relative macroscopic brittleness of some glasses was correlated to instability of their silica network. It was shown, for Borofloat and N-ZK7, that Si-O-Si angle reduced under irradiation and that there was a creation of three-membered rings. These two phenomena were correlated in the previous study to their macroscopic shrinking, and breaking in case of heterogeneous irradiation. Such features were not observed on the two other glasses. The results here presented come from Magic Angle Spinning Nuclear Magnetic Resonance spectroscopy (MAS NMR) and Small Angle Neutron Scattering measurement (SANS). The aims were to gather informations on glass structure evolution under irradiation at inter-atomic and nanometre scale, respectively, and to combine them to the ones previously obtained from Raman spectroscopy.

2. Materials and methods

2.1. Studied glasses

Four industry-grade alkali-borosilicate standards were studied, namely Borofloat, N-ZK7, N-BK7 and S-BSL7. The first three are commonly used for neutron guide manufacturing. In all cases, glass samples were provided by different neutron guide manufacturers. As far as sample sizes are concerned, the powder used for NMR experiments came from specimens with an initial dimension of $10 \times 10 \times 1.1$ mm^3, and for the SANS experiments they were measuring $10 \times 10 \times 0.3$ mm^3. The chemical composition of these glasses is listed in Table 1. The relative amount of four-fold coordinated boron atoms, BO_4^-, and their speciation between (4Si, 0B) and (3Si, 1B) sites are reported in Table 2. Estimation of N4 has been done using Dell and Bray model [28]. Two situations were assumed : existence of solely alkali, boron, and silicon species, $N4_{ABS}$,

Table 1
Chemical composition of the studied glasses.

mol.%	Borofloat	N-ZK7	N-BK7	S-BSL7
SiO_2	82	66	73	73.5
B_2O_3	12	11.5	10	9.5
ZnO		10		
Al_2O_3	1.5	4	0.25	
MgO			1.25	
Na_2O	4	7.5	10	10
K_2O	0.5		5	5.5
CaO		1	0.25	
BaO			0.25	0.5

Table 2
Relative amount of four-fold coordinated boron atoms (N4) and their speciation infered from 18.8 T measurements [27]. Values in percent.

	$N4_{ABS}$	$N4_{real}$	$N4_{measured}$	BO_4^-(0B, 4Si)	BO_4^-(1B, 3Si)
Borofloat	36	22	23	32	68
N-ZK7	63	48	30	4	96
N-BK7	95	95	91	65	35
S-BSL7	97	97	90	65	35

Table 3
Proportion of non-bridging oxygen (NBO) per silicon atom, estimated from remaining network formers.

Zn and Mg charge compensation	NBO (%)	
	no	yes
Borofloat	0.3	0.3
N-ZK7	1.6	-1.4
N-BK7	8	7
S-BSL7	10	9

or accounting every oxide that could generate BO_4^- or incorporate network modifiers, $N4_{real}$. It should be mentioned that all glasses, according to Dell and Bray model have :

$$K = \frac{[SiO_2]}{[B_2O_3]} < 8 \quad (1)$$

Analysis of Dell and Bray values show that, for N-BK7 and S-BSL7, the excess of network modifiers should moderate intermediate ions, which is what is observed with measured N4. For Borofloat, one might think that, as its composition is relatively short and the behaviour of alumina in sodium borosilicate is well understood [29], the BO_4^- content should be similar to predicted $N4_{real}$ value. Finally, negative $N4_{real}$ value for N-ZK7 tells us that Dell and Bray model cannot be used for that glass since the content of intermediate ions, Zn, Mg or AL, is higher than network modifiers. Experimental values, $N4_{measured}$, are extracted from the MAS NMR signals, published in a previous study [27], acquired on a 18.8 T machine.

One can estimate the number of non-bridging oxygen (NBO) per silicon atoms from measured N4 values. This can be carried out by means of the following expression,

$$NBO = \frac{[Na_2O] + [K_2O] + [CaO] + [BaO] - N4 \times [B_2O_3] - [Al_2O_3] - ([ZnO] + [MgO])}{[SiO2]} \quad (2)$$

which takes into account network modifiers not used by the boron atoms from where one has to subtract the alumina content. An extreme case can be figured out by considering that MgO and ZnO will be preferentially charge compensated. Table 3 reports the results of these calculations. Value for N-ZK7 in the case of a full charge compensation of zinc oxide confirms the complexity of this glass. As observed will be observed from the STEM atom mapping,

Table 4
Informations on thermal neutron irradiation in T4 tube (ILL) and damages induced by $^{10}B(n,\alpha)^{7}Li$. Perturbed flux measured on sample surface by zirconium foil activation.

Sample thickness	$\phi_{unperturbed}$	$\phi_{perturbed}$	α particle		Li recoil nuclei	
(mm)	(n/cm^2/s)	(n/cm^2/s)	Displaced atoms (ion^{-1})	range (μm)	Displaced atoms (ion^{-1})	range (μm)
0.3	2×10^{13}	1.5×10^{13}	160	4.5 – 5	400	2.4 – 2.6
1.1		0.7×10^{13}				

Table 5
Thermal neutron irradiation doses and corresponding deposited energy by ionisation and nuclear interactions.

Dose	NMR	SANS
Fluence (n/cm^2)	3.9×10^{17}	7.9×10^{17}
$^{10}B(n,\alpha)^{7}Li$ reactions (/cm^3)	1.5×10^{18}	3.1×10^{18}
$E_{ioniz.}$ (keV/cm^3)	3.5×10^{21}	7.3×10^{21}
$E_{nucl.}$ (keV/cm^3)	5.1×10^{19}	1.0×10^{20}
dpa	0.012	0.025

zinc rich zones concentrate sodium. However, considering their relative amount, zinc is not fully in four-fold coordination.

2.2. Irradiation method

Thermal neutron irradiations have been carried out in the T4 tube at ILL that provides an unperturbed thermal flux of 2×10^{13} n/cm^2/s. More details on the irradiation conditions are given in [22]. Table 4 summarizes the irradiation characteristics and damages induced by the $^{10}B(n, \alpha)^{7}Li$ reactions. Sample maximum temperature has been estimated considering the worst case scenario of an irradiation shuttle fully loaded with 1.1 mm thick samples, without flux perturbation due to $^{10}B(n, \alpha)^{7}Li$ reactions, and cooling with solely conduction to surrounding water. It yielded a maximum temperature around 65 °C [22], which is low enough to avoid thermal effects on the vitreous structure. Table 5 reports the neutron doses that NMR and SANS samples were exposed to and the associated damages estimated by SRIM [30].

2.3. Characterization techniques

2.3.1. Electronic Microscopy

A set of measurements using a Transmission Electron Microscope (TEM) were carried out. Observations were performed using a MET LaB6 JEM-2010. As N-ZK7 show electronic contrast, Scanning Transmission Electron Microscope (STEM) observations were done on that glass with a Jeol 2100F-200 kV FEG machine. These analysis were done on pristine samples only.

2.3.2. Small-Angle Neutron Scattering

Small Angle Neutron Scattering measurements were done at the ILL D11 instrument [31,32]. Beam wavelength was set to 6 Å and its diameter to 7 mm. Data shown in the result section comes from measurements acquired with the detector located at 1.5, 8 and 20 m from sample position. Since solid samples were available, all four glasses were analysed. This gave the opportunity to measure structural informations that could not be detected in a previous work [27] where powder samples were used. SANS curve analysis mentioned in this work was done with SASview software [33].

2.3.3. Nuclear Magnetic Resonance

Pristine samples were analysed at UCCS-UGSF Lille on a 18.8 T spectrometer [27]. Considering irradiated samples, all the experiments were conducted at JRC-Karlsruhe on a 400 MHz (9.4 T) spectrometer dedicated to the analysis of nuclear and irradiated materials [34]. They were conducted using a 1.3 mm Bruker MAS probe and the rotors were spun at 40 kHz at the Larmor frequencies of 128.378, 79.495 and 105.842 MHz for ^{11}B, ^{29}Si and ^{23}Na respectively. A short pulse length ($\pi/12$, pulse duration of 0.3 μs) was used to ensure a quantitative spectrum with repetition times of up to 10 s for ^{11}B and 1 s for ^{23}Na. ^{29}Si MAS NMR experiments were acquired using a CPMG pulse sequence [35] using the recycling delays put in Table 6. The position of the ^{29}Si peak was determined by considering its barycentre. All spectra were referenced to external samples of 1 M boric acid solution (^{11}B, 19.6 ppm), 1 M NaCl solution (^{23}Na, 0 ppm) and 1 M TMS solution (^{29}Si, 0 ppm). MAS NMR spectra were fitted using the DMfit software[36].

Table 6
Recycling delays (RD) used to acquire the ^{29}Si CPMG MAS NMR experiments.

	Pristine	Irradiated
Borofloat	100	20
S-BSL7	100	100

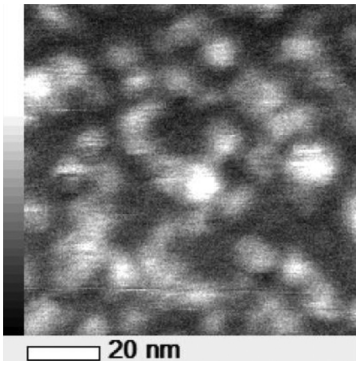

Fig. 1. N-ZK7 STEM-HAADF image.

3. Results

3.1. STEM

The recorded STEM High-Angle Annular Dark Field (HAADF) image of N-ZK7 is reported in Fig. 1. Contrary to TEM image, electronically heavier regions are white with STEM-HAADF technique. Chemical analysis of this image is reported in Fig. 2 and Fig. 3, where one can see that these aggregates are made of zinc and sodium. Chemical mapping of boron, silicon and aluminium are not reported here as they did not show specific fluctuations. A concentration analysis was carried out using ImageJ software [37] on a 20 nm band height vertically centered on Fig. 1. Concentration profiles are gathered in Fig. 4 where one can see phase segregation concerns especially zinc and sodium, and to a lower level aluminium. Sodium oxide serves as charge compensator in these aggregates [38,39]. Silicon and boron are not affected at this scale.

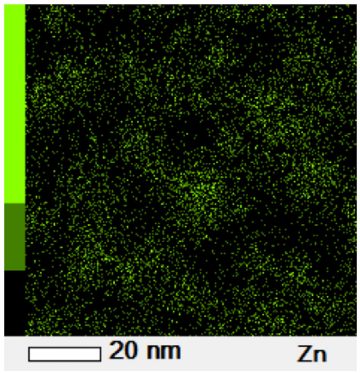

Fig. 2. N-ZK7 Zn concentration analysis from Fig. 1.

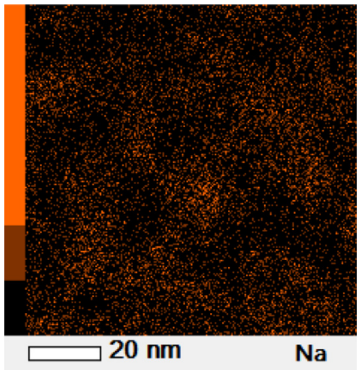

Fig. 3. N-ZK7 Na concentration analysis from Fig. 1.

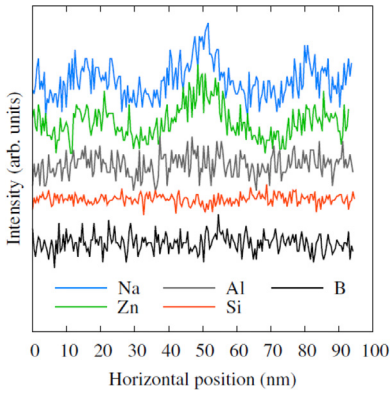

Fig. 4. N-ZK7 concentration profiles extracted from Fig. 1 on a 20 nm height band vertically centered.(top to bottom: Na, Zn, Al, Si, B).

3.2. SANS measurements

Scattering intensity of the four glasses are gathered in Fig. 5. One can observe that Borofloat and N-ZK7 exhibit noticeable features such as a broad intensity band around 0.08 $Å^{-1}$ and a peak around 0.03 $Å^{-1}$, respectively. All materials, at low momentum transfer, show an intensity ramp that increases with decreasing Q.

The effects of thermal neutron irradiation on scattering intensity are reported in Fig. 6, 7, 8, and 9. On each plot, one can see pristine and irradiated states intensities, and their ratio. For Borofloat, one can see a shift of the band toward higher momentum transfer. Concerning N-ZK7, the peak is also shifted to higher Q while the intensity of the low Q ramp is decreased. N-BK7 and S-BSL7 curves show a similar behaviour: their intensity is decreased on the whole study range and appears to be more marked between 0.006 $Å^{-1}$ and 0.1 $Å^{-1}$.

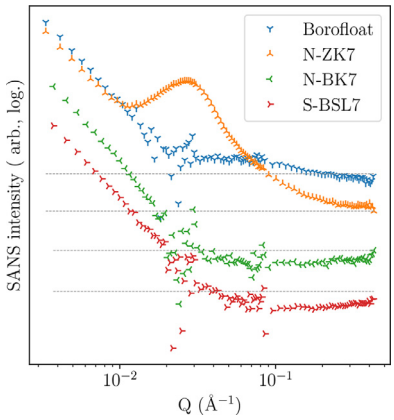

Fig. 5. SANS intensity from pristine samples.

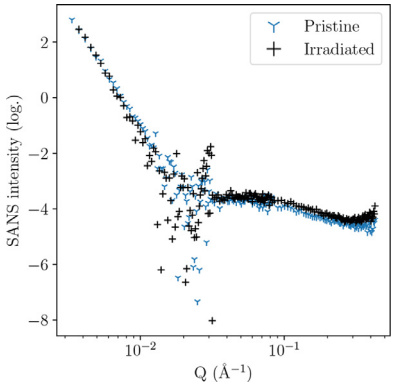

Fig. 6. Borofloat SANS intensity before and after irradiation.

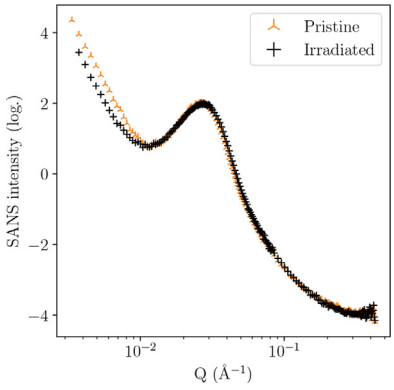

Fig. 7. N-ZK7 SANS intensity before and after irradiation.

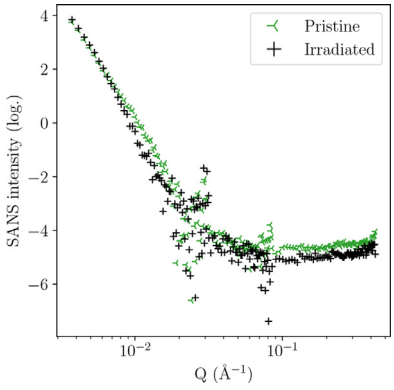

Fig. 8. N-BK7 SANS intensity before and after irradiation.

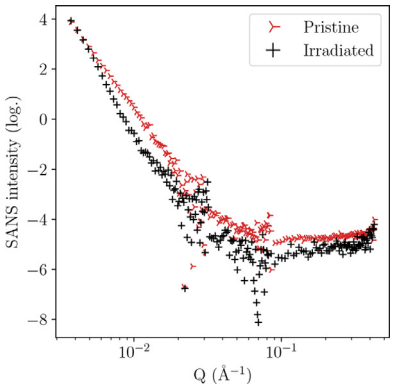

Fig. 9. S-BSL7 SANS intensity before and after irradiation.

Table 7
Exponential slopes derived at low-Q (< 10^{-2} Å^{-1}).

	Pristine	Irradiated
Borofloat	3.54 ± 0.05	3.95 ± 0.08
N-ZK7	3.13 ± 0.02	3.31 ± 0.03
N-BK7	3.67 ± 0.02	4.25 ± 0.05
S-BSL7	3.60 ± 0.02	4.69 ± 0.02

For Q-value below around 10^{-2} Å^{-1}, intensity curves of the different glasses in both states have been fitted with a power law function,

$$I(Q) = a \times Q^{-p} + b \quad (3)$$

Where a stands for a scaling factor, p for the power law exponent, and b the background. Fitted p parameters are gathered in Table 7.

A Guinier fit was done for Borofloat on the broad intensity band around 0.08 Å^{-1} with a function,

$$I(Q) = a \exp\left(\frac{-r_g^2 Q^2}{3}\right) + b \quad (4)$$

where r_g is the gyration radius [40], a and b are fitting parameters. The analysis was done for $Q \in [3 \times 10^{-2} \ ; \ 30 \times 10^{-2}]$ Å^{-1}. It yielded a gyration radius of 13.5 ± 0.4 Å for the pristine state that decreases to 11.8 ± 0.3 Å after irradiation.

The peak position of N-ZK7 and its shift under irradiation was obtained by fitting the SANS signal with a Gaussian function between 16×10^{-3} and 43×10^{-3} Å^{-1}. It gave a peak around 0.0264 Å^{-1} before irradiation that drifts to 0.0272 Å^{-1} after, with associated uncertainties below 2×10^{-5} Å^{-1}.

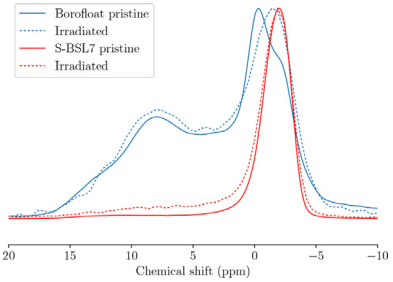

Fig. 10. ^{11}B MAS NMR spectra. $B_0 = 9.4$ T.

Table 8
BO_4^- proportion (N4) determined from the fitting of the ^{11}B MAS NMR spectra.

	Pristine	Irradiated
Borofloat	23 %	21 %
S-BSL7	88 %	78 %

3.3. MAS NMR

For the Borofloat glass, the ^{11}B MAS NMR spectrum acquired before and after irradiation is gathered in Fig. 10 and Fig. 11, respectively. Spectra of the non-irradiated samples acquired at 18.8 T was previously published in [27]. We used here the same set of fitting parameters. Two main peaks corresponding to the BO_3 and BO_4^- units are identified. It is possible to differentiate for the two magnetic field the two peaks corresponding to i) four-fold coordinated boron atom linked to four silicon atoms (BO_4^-(0B, 4Si)) at −1.9 ppm and ii) four-fold coordinated boron linked to three silicon and one boron atoms (BO_4^-(1B, 3Si)) at 0.2 ppm [26]. The BO_4^- amount before and after irradiation have been put in Table 8. While almost no variation of the BO_4^- and BO_3 content is detected for the borofloat glass after irradiation, we have detected a change in the BO_4^-(0B, 4Si) and BO_4^-(1B, 3Si) content. In fact, before irradiation and with the 9.4 T NMR measurement, we determined

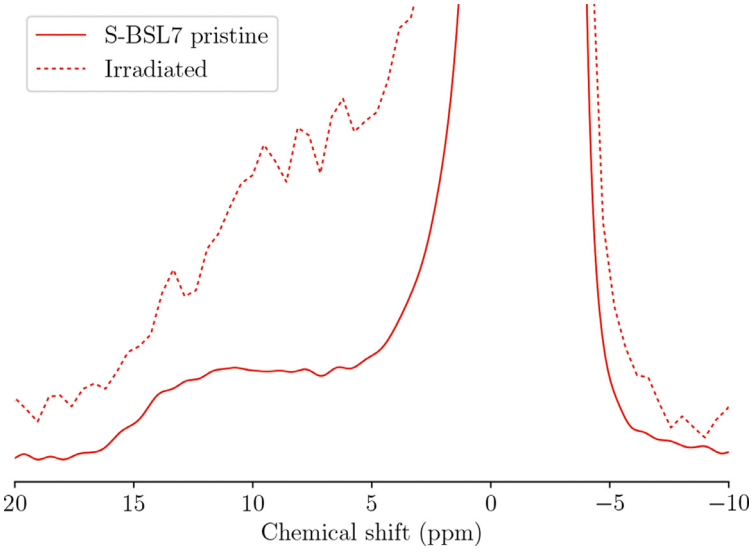

Fig. 11. ^{11}B MAS NMR spectra from S-BSL7. Zoom on BO_3 population. $B_0 = 9.4$ T.

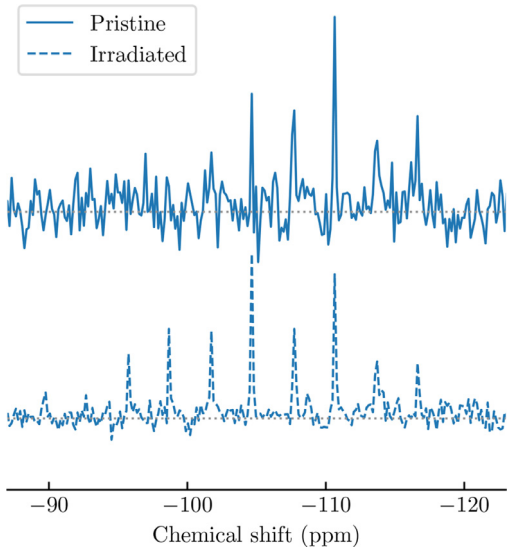

Fig. 12. ^{29}Si CPMG MAS NMR spectra from Borofloat. $B_0 = 9.4$ T.

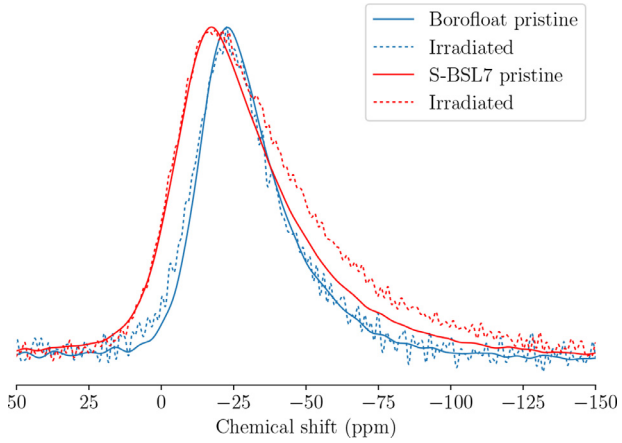

Fig. 13. ^{23}Na MAS NMR spectra. $B_0 = 9.4$ T.

BO_4^-(0B, 4Si) = 11 % and BO_4^-(1B, 3Si) = 13 % and after BO_4^-(0B, 4Si) = 19 % and BO_4^-(1B, 3Si) = 5.2 %. The present observation underlines that ^{10}B(n,α)^{7}Li reactions, through ballistic mixing, break up BO_4^-–BO_4^- pairs and distribute them homogeneously within the silica network. Also, this observation points in the direction of the formation of B-O-Si linkages. As Nanba *et al.* [41] have shown that the silica network is influenced by the presence of boron in its network by a shift in the ^{29}Si peak toward higher chemical shifts we found relevant to also acquire ^{29}Si CPMG MAS NMR. The results are presented in Fig. 12. The ^{29}Si peak is found at −108.8 ppm before irradiation and at −106.6 ppm after irradiation. This behaviour is positively in agreement with the BO_4^- variations previously mentioned. Similar variation of the ^{29}Si signal under swift heavy ion irradiation was observed [42]. To complete this study about the effect of irradiation on the local structure of the Borofloat glass, we performed ^{23}Na MAS NMR with the spectra presented in Fig. 13. Their analysis is reported in Table 9. No main differences where observed between the pristine and the irradiated ^{23}Na MAS NMR spectra which might confirm that there is a fewer modification of the BO_3 network.

^{23}Na MAS NMR spectra main difference between the two glasses is the drift toward higher shift for S-BSL7, which contains relatively more sodium. Such a displacement of the sodium peak has been related to its structural role in the glass network [43].

Table 9
^{23}Na NMR shift (δ_{iso}) and quadrupolar coupling constant (C_Q) obtained after fitting of the spectra.

	δ_{iso} (ppm)	C_Q (MHz)
Borofloat, pristine	−11.9	2.7
Borofloat, irradiated	−10.6	2.7
S-BSL7, pristine	−2.7	3.1
S-BSL7, irradiated	−1.2	3.6

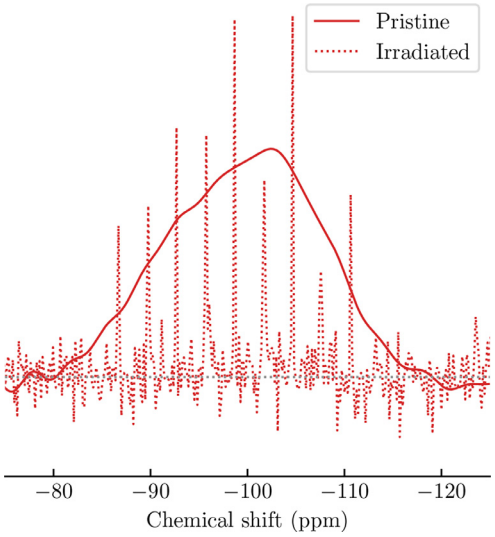

Fig. 14. ^{29}Si CPMG MAS NMR spectra from S-BSL7. $B_0 = 9.4$ T.

This chemical element would act more as a network modifier than a charge compensator in the case of S-BSL7 than for Borofloat. This is coherent since, for Borofloat and N-ZK7, sodium is mainly used as charge compensator, while N-BK7 and S-BSL7 has sufficiently enough alkali for having most of the boron in four-fold coordination, and the excess of alkali is used to create NBOs.

For the non irradiated S-BSL7 glass, both BO_3 and BO_4^- species are also present (Fig. 10). The BO_3 content of 10 % is much lower than for the non irradiated borofloat glass. No distinction between the BO_4^-(0B, 4Si) and BO_4^-(1B, 3Si) species was this time possible at the two magnetic fields. After irradiation, there is a slight increase of the BO_3 species as can be seen on Fig. 11 and the extracted N4 value reported in Table 8. By comparing the ^{29}Si MAS NMR spectra, Fig. 14, no main variation of the peak barycentre is detected with ^{29}Si chemical shift at −99.5 ppm for the pristine and −99.7 ppm for the irradiated glass. Considering the speciation of BO_4^- units, irradiation does not seem to involve drastic conversions from BO_4^-(0B, 4Si) to BO_4^-(1B, 3Si) compared with what was previously described for the borofloat glass. Finally, we also acquired the ^{23}Na MAS NMR of the sample. Irradiation leads to a broadening of the ^{23}Na peak with a C_Q increasing from 3.6 kHz to 3.1 kHz. This line broadening effects were previously attributed to an increase of the disorder around Na (mainly its oxygen first-coordination sphere) and a shortening of the average Na-O distance. Sodium being thus here more network modifier than charge compensator [43]. This is in agreement with the decrease of BO_4^- amount which corresponds to a release of charge compensators from boron to silicon environment were they act as network modifier. Here, our result showing that irradiation induces a modification of both the BO_3 and ^{23}Na network, is in some ways analogous to findings reported on borosilicate glass irradiated with xenon ions (fluence 3×10^{13} ions cm-2) [21] or ^{10}B(n, α)^{7}Li (fluence 5.2×10^{19} ions/cm2) [44] or swift heavy ions (fluence 3×10^{13} ions/cm2) [42].

4. Discussion

4.1. Large scale structures

All glasses show a noticeable increase of the slope at low-Q. It indicates the conversion of surface-fractal interfaces into mass fractal. Considering measurements made on the same samples but in powder, the intensity in that region has considerably been reduced using solid samples [27]. Also, the fact that it is affected by irradiation means that it carries information on the vitreous "network" itself and not solely the surface. In a further study, using mirror polished sample should allow to diminish even more the signal coming from samples' surface.

N-BK7 and S-BSL7 SANS curves have a similar evolution under neutron flux. On the whole Q-range, intensity decreases which could be related to an attenuation of the background. As noted in Table 7, the slope appears to increase of at least 15 % for both glasses when it is fitted by one function. However, one can remark an inflexion point around 0.008 $Å^{-1}$. From that, one could support the use of two power laws to fit the curve. As an example, for irradiated N-BK7, it is possible to fit data with a set of p parameters equal to 3.7 and 5.2 with a crossover location found around 0.007 $Å^{-1}$. Such an analysis would suggest that $^{10}B(n, \alpha)^7Li$ reaction induce a coexistence of surface-fractal and mass-fractal interfaces. This type of feature may be hinted for Borofloat, from the slight curve infliction in the same Q-region.

SANS signal of Borofloat shows two remarkable features : the low-Q ramp, that corresponds to Porod's law, and the broad intensity band at higher Q, that corresponds to a Guinier regime. Due to its relatively low content in alkali, Borofloat's vitreous network is characterized by alkali-borate-rich areas intermingled with a silica-rich phase. The noticeable decrease under irradiation of the gyration radius from 13.5 ± 0.4 Å to 11.8 ± 0.3 Å could be related to the compaction of the silica-rich phase. Such a trend has been detected with Raman spectroscopy on that glass from decrease of Si-O-Si angle and increase of three-membered rings [27]. A fit with a power law for $Q \geqslant 0.1$ Å yields a p parameter around 1.3. This corresponds to elongated structures [45,46] which is what has been observed for glass of similar composition [47]. A fit using a cylindrical model was intended but without success to extract significant informations. However, it has to be noted that compared to a preceding study on Borofloat, the use of thin solid samples allowed to detect the existence of a Guinier regime. A deeper analysis could require even thinner samples, if technically possible, and different level of fluence. The later parameter should allow to validate, or not, if the variation of the gyration radius is related to the compaction of the silica-rich phase. Finally, one can notice that there is no significant decrease of intensity due to irradiation. This means that the phases detected before irradiation are not noticeably blended because of irradiation.

The remarkable feature for N-ZK7 is the structure peak located around 0.026 $Å^{-1}$ that shifts to a higher value due to irradiation. This signs the existence of aggregates and the peak position can be related to the distance between them. STEM imaging on that glass demonstrated the existence zinc-alkali-rich areas with spherical shape, typical diameter between 10 and 30 nm, and centre-to-centre distance between 20 and 30 nm. Application of Bragg's law on the structure peaks yields a distance between the aggregates of 23.8 nm and 23.0 nm before and after irradiation, respectively. Such dimensions are comparable with what has been obtained by STEM imaging. One can notice a peak in the ratio curve around 0.09 $Å^{-1}$. However, since it corresponds to the junction between two detectors positions (1.5 and 8 m), as one can see from the change in binning density, that peak probably does not contain significant informations. Considering the composition of N-ZK7, the silicon-boron phase separation should also feature a Guinier regime as it has been detected for Borofloat. However, considering the intensity and width of the broad structure peak, one can estimate that the Guinier regime could be hidden in the peak.

4.2. Borosilicate network

The modification of BO_4^- speciation detected by MAS NMR does not seem to drive glass macroscopic evolution of Borofloat for a fluence below 5×10^{17} n/cm^2. Indeed, it was shown for such a borosilicate, with a rather low content in network modifier, that its behaviour is dominated by its silica network [27]. As irradiation appears to improve the incorporation of boron into the silica network, it should stabilize it, as it is the case for S-BSL7 and N-BK7. Though, considering what has been observed macroscopically, this effect is negligible with respect to the compaction of the silica network. Also, one should expect to see the appearance of a reedmergnerite-like signal on its Raman spectra, which was not the case [27]. The higher macroscopic stability of N-ZK7 compared to Borofloat, that shrinks up to 1 % compared to 2 %, might be explained by the larger amount of four-fold coordinated boron atoms. These are either incorporated as reedmergnerite-like or danburite-like structures, whether they are detected as BO_4^-(0B, 4Si) or BO_4^-(1B, 3Si) units with NMR [25]. In the Raman spectra previously published, [27], one can see that the drift of Si-O-Si peak, corresponding to Si-O-Si angle decrease, is smaller for N-ZK7 than for Borofloat. Both glasses seem to converge toward the same Raman shift, though N-ZK7 is more compact at pristine state than Borofloat.

The behaviour of S-BSL7 under irradiation can be compared to the one of homogeneous borosilicate glasses, such as the R7T7 [7], that swells due to irradiation. A similar behaviour in BO_3/BO_4^- proportion has also been observed for that glass [7,13]. A study on sodium-borosilicate irradiated with krypton and xenon ions has also shown that BO_4^- units were converted into BO_3 and a non-bridging oxygen (NBO) [42]. It was shown that this NBO should induce a depolymerization of the silica network. This was not specially observed on S-BSL7 ^{29}Si MAS NMR measurement. Considering the fact that BO_3 is more stable at high temperature [48,49], it seems that $^{10}B(n, \alpha)^7Li$ reactions drive S-BSL7 toward a structure that corresponds to a higher fictive temperature. Since glass melts density are inversely correlated to their temperature such a modification of boron speciation allows to understand glass' swelling under irradiation. This is coherent with studies that compared ion irradiation effect to the one induced by fast quenching [16,21].

It appears that a low amount of alkali in a borosilicate favours the existence of a silica-rich phase which behaviour dominates the one of the whole glass. On the contrary, a sufficient amount of alkali to have mainly BO_4^- units permits their assembly with silicon in reedmergnerite-like structures and generates a glass which behaviour under irradiation is linked to fictive temperature considerations.

5. Conclusion

SANS measurements allowed to detect the silica-rich phase contraction under irradiation of alkali-poor borosilicate glasses, such as Borofloat and N-ZK7. This information confirms that the bulk behaviour is dominated by the silica-rich domain. For N-ZK7, zinc-sodium rich aggregates were detected with SANS and observed with STEM imaging. Boron speciation of Borofloat is not specifically modified by irradiation : the proportions between BO_3 and BO_4^- is stable. However the specific BO_4^- speciation under irradiation favours BO_4^-(4Si, 0B) units which corresponds to boron atoms more homegeneously distributed. This had not been detected in a previous paper with Raman analysis from appearance of a reedmergnerite peak with irradiation.

This study calls for the production of glasses with fixed boron-oxide content and variable alkali / silica ratio. There analysis by SANS could possibly show the disappearance of the Guinier feature that reveal the existence of phase segregation.

Alkali-rich borosilicate, such as N-BK7 or S-BSL7, did not show noticeable variations of their SANS signal due to $^{10}B(n, \alpha)^{7}Li$ reactions. This suggests a stability of their homogeneity to irradiation. MAS NMR analysis has shown that glasses structure is driven toward higher fictive temperature as marked by the conversion of four-fold to three-fold coordinated boron atoms. This can be correlated to glass swelling under irradiation.

While Raman analysis from a previous paper show silica network behaviour under irradiation, MAS NMR allowed here to extract specific information on boron environment. Both techniques are complementary to study alkali borosilicate glasses under irradiation.

Declaration of Competing Interest

The authors declare that they have no known competing financial interests or personal relationships that could have appeared to influence the work reported in this paper.

CRediT authorship contribution statement

R. Boffy: Investigation, Resources, Formal analysis, Writing - original draft. **L. Martel:** Investigation, Formal analysis, Writing - original draft, Writing - review & editing. **R. Schweins:** Writing - review & editing. **J. Somers:** Project administration. **J. Beaucour:** Supervision. **F.J. Bermejo:** Supervision.

Acknowledgments

Financial support from the IR-RMN-THC Fr3050 CNRS for conducting the research is gratefully acknowledged. This work benefited from the use of the SasView application, originally developed under NSF award DMR-0520547. SasView contains code developed with funding from the European Union's Horizon 2020 research and innovation programme under the SINE2020 project, grant agreement № 654000. We would like to thank the guide manufacturers for the assistance they provided throughout this study. Romain Boffy acknowledges financial support from the ESS-Bilbao Consortium. Finally, the study here exposed would not have been possible without the combined efforts of ILL staff throughout several years, specially the SMAE, BPC, Bloc-Pile and Radio-Protection services. The authors thank them for their constant support.

Supplementary material

Supplementary material associated with this article can be found, in the online version, at doi:10.1016/j.jnucmat.2020.152699.

References

[1] U. Schmidt, D. Dubbers, K. Raum, O. Joeres, O. Scharpf, Supermirror beam bender and concentrator for slow neutrons, Journal of Neutron Research 5 (1996) 81–88.
[2] B. Ballot, A. Menelle, J. Mimault, T. Girardeau, F. Samuel, K. Al Usta, Titanium Evolution and Nickel Restoration Under Neutron Irradiation in Ni/Ti Multilayers, J. Phys. IV 05 (C3) (1995), doi:10.1051/jp4:1995331. C3–305–C3–310
[3] J. Rowe, Analysis of the causes and consequences of neutron guide tube failures, Joint meeting of the National Organization of Test, Research, and Training Reactors and the International Group on Research Reactors, 2005.
[4] P. Link, Neutron guides, not always perfect, FRM II News 8 (2012) 10.
[5] S. Pullen, G. Davidson, S. Pangalis, F. Klose, S. Kennedy, Report on the repair of the OPAL neutron beam transport system, Joint IGORR 2013 and IAEA Technology Meeting, 2013.
[6] S. Peuget, J.-N. Cachia, C. Jégou, X. Deschanels, D. Roudil, V. Broudic, J.-M. Bart, Irradiation stability of R7T7-type borosilicate glass, Journal of nuclear materials 354 (2006) 1–13.
[7] S. Peuget, J.-M. Delaye, C. Jégou, Specific outcomes of the research on the radiation stability of the french nuclear glass towards alpha decay accumulation, Journal of Nuclear Materials 444 (2014) 76–91.
[8] S. Gin, P. Jollivet, M. Tribet, S. Peuget, S. Schuller, Radionuclides containment in nuclear glasses: an overview, Radiochimica Acta 105 (11) (2017) 927–959, doi:10.1515/ract-2016-2658.
[9] K. Sun, L.M. Wang, R.C. Ewing, W.J. Weber, Electron irradiation induced phase separation in a sodium borosilicate glass, Nucl. Instrum. Methods Phys. Res., Sect. B 218 (2004) 368–374, doi:10.1016/j.nimb.2003.12.022. Proceedings of the Twelfth International Conference on Radiation Effects in Insulators
[10] N. Ollier, G. Rizza, B. Boizot, G. Petite, Effects of temperature and flux on oxygen bubble formation in Li borosilicate glass under electron beam irradiation, Journal of Applied Physics 99 (7) (2006).
[11] G. Möbus, M. Ojovan, S. Cook, J. Tsai, G. Yang, Nano-scale quasi-melting of alkali-borosilicate glasses under electron irradiation, Journal of Nuclear Materials 396 (2) (2010) 264–271, doi:10.1016/j.jnucmat.2009.11.020.
[12] K.J. Yang, T.S. Wang, G.F. Zhang, H.B. Peng, L. Chen, L.M. Zhang, C.X. Li, F. Tian, W. Yuan, Study of irradiation damage in borosilicate glass induced by he ions and electrons, Nucl. Instrum. Methods Phys. Res., Sect. B 307 (2013) 541–544, doi:10.1016/j.nimb.2012.12.113. The 18th International Conference on Ion Beam Modifications of Materials (IBMM2012)
[13] A.H. Mir, B. Boizot, T. Charpentier, M. Gennisson, M. Odorico, R. Podor, C.J. egou, S. Bouffard, S. Peuget, Surface and bulk electron irradiation effects in simple and complex glasses, J. Non-Cryst. Solids 43 (141–149) (2016).
[14] C. Mylonas, R. Truell, Radiation effects from (n,α) reactions in boron glass and energy of the racting neutrons, Journal of applied physics (1958).
[15] K. N'Guy-Maréchal, Tenue sous irradiation de supermiroirs pour guides de neutrons, Université Paris Sud - Paris XI, 1997 Theses.
[16] E.A. Maugeri, S. Peuget, D. Staicu, A. Zappia, C. Jegou, T. Wiss, Calorimetric study of glass structure modification induced by alpha decay, Journal of the American Ceramic Society 95 (9) (2012) 2869–2875, doi:10.1111/j.1551-2916.2012.05304.x.
[17] K.B. Patel, S. Peuget, S. Schuller, G.I. Lampronti, S.P. Facq, C. Grygiel, I. Monnet, I. Farnan, Discovery of a maximum damage structure for Xe-irradiated borosilicate glass ceramics containing powellite, Journal of Nuclear Materials 510 (2018) 229–242, doi:10.1016/j.jnucmat.2018.08.012.
[18] A.H. Mir, I. Monnet, B. Boizot, C. Jégou, S. Peuget, Electron and electron-ion sequential irradiation of borosilicate glasses: Impact of the pre-existing defects, Journal of Nuclear Materials 489 (2017) 91–98, doi:10.1016/j.jnucmat.2017.03.047.
[19] R. Kaur, S. Singh, O.P. Pandey, Modifications induced in the structural and optical properties of bismuth sodium borosilicate glass thin films by 120 MeV Ag^{7+} ions, Nucl. Instr. and Meth. in Phys. Res. B (2013).
[20] P. Lv, L. Chen, B.T. Zhang, W. Yuan, B.H. Duan, Y.D. Guan, Y. Zhao, X.Y. Zhang, L.M. Zhang, T.S. Wang, Composition-dependent mechanical property changes in au-ion-irradiated borosilicate glasses, Journal of Nuclear Materials 520 (2019) 218–225, doi:10.1016/j.jnucmat.2019.04.025.
[21] S. Peuget, E.A. Maugeri, T. Charpentier, C. Mendoza, M. Moskura, T. Fares, O. Bouty, C. Jégou, Comparison of radiation and quenching rate effects on the structure of a sodium borosilicate glass, Journal of Non-Crystalline Solids 378 (2013) 201–212.
[22] R. Boffy, M. Kreuz, J. Beaucour, U. Köster, F.J. Bermejo, Why neutron guides may end up breaking down? Some results on the macroscopic behaviour of alkali-borosilicate glass support plates under neutron irradiation, Nucl. Instrum. Methods Phys. Res., Sect. B 358 (2015) 179–187, doi:10.1016/j.nimb.2015.06.017.
[23] A. Wright, B. Bachra, T. Brunier, R. Sinclair, L. Gladden, R. Portsmouth, A neutron diffraction and MAS-NMR study of the structure of fast neutron irradiated vitreous silica, Journal of Non-Crystalline Solids 150 (1992) 69–75.
[24] R. Boffy, T. Bigault, J. Beaucour, F.J. Bermejo, Irradiation induced stresses in alkali-borosilicate glasses: experimental characterization and finite element analysis, Journal of Neutron Research 18 (4) (2015) 99–107, doi:10.3233/JNR-160028.
[25] D. Manara, A. Grandjean, D.R. Neuville, Advances in understanding the structure of borosilicate glasses: A Raman spectroscopy study, American Mineralogist 94 (2009) 777–784.
[26] F. Angeli, T. Charpentier, D. de Ligny, B. Cailleteau, Boron speciation in soda-lime borosilicate glasses containing zirconium, Journal of American Ceramic Society 93 (9) (2010) 2693–2704.
[27] R. Boffy, S. Peuget, R. Schweins, J. Beaucour, F.J. Bermejo, High thermal neutron flux effects on structural and macroscopic properties of alkali-borosilicate glasses used as neutron guide substrate, Nucl. Instrum. Methods Phys. Res., Sect. B 374 (2016) 14–19, doi:10.1016/j.nimb.2015.10.011.
[28] W.J. Dell, P.J. Bray, S.Z. Xiao, ^{11}B NMR studies and structural modeling of Na_2O – Bsbs$2O_3$–SiO_2 glasses of high soda content, Journal of Non-Crystalline Solids 58 (1983) 1–16.
[29] G. El-Damrawi, W. Müller Warmuth, H. Doweidar, I. Gohar, 11B, 29Si and 27Al nuclear magnetic resonnance studies of Na_2O–Al_2O_3–B_2O_3–SiO_2 glasses, Physics and Chemistry of Glasses 34 (2) (1993) 52–57.
[30] J. Ziegler, J. Manoyan, The stopping of ions in compounds, Nucl. Instrum. Methods Phys. Res., Sect. B 35 (1988) 215–228.

[31] P. Lindner, R. Schweins, ILL Technical Report, Technical Report, ILL, 2006.
[32] K. Lieutenant, P. Lindner, R. Gaehler, A new design for the standard pinhole small-angle neutron scattering instrument D11, Journal of Applied Crystallography 40 (2007) 1056–1063.
[33] SasView, (http://www.sasview.org/).
[34] L. Martel, J. Somers, C. Berkmann, F. Koepp, A. Rothermel, O. Pauvert, C. Selfslag, Farnan 84.
[35] F.H. Larsen, I. Farnan, 29Si and 17O (Q)CPMG-MAS solid-state NMR experiments as an optimum approach for half-integer nuclei having long T1 relaxation times, Chemical Physics Letters 357 (5) (2002) 403–408, doi:10.1016/S0009-2614(02)00520-1.
[36] D. Massiot, F. Fayon, M. Capron, I. King, S.L. Calvé, B. Alonso, J.-O. Durand, B. Bujoli, Z. Gan, G. Hoatson, Modelling one- and two-dimensional solid-state NMR spectra, Magnetic Resonance in Chemistry 40 (2002) 70–76.
[37] C. Schneider, W. Rasband, K. Eliceiri, NIH image to ImageJ: 25 years of image analysis. 9(7) (????) 671–675. 10.1038/nmeth.2089
[38] J.C. Hurt, C.J. Phillips, Structural role of zinc oxide in glasses in the system Na_2O - ZnO - SiO_2, Journal of the American Ceramic Society 53 (5) (1971) 269–273.
[39] A.B. Rosenthal, S.H. Garofalini, Structural role of zinc oxide in silica and soda-silica glasses, Journal of American Ceramic Society 70 (11) (1987) 821–826.
[40] A. Guinier, G. Fournet, Small-angle scattering of X-Rays, John Wiley and Sons, 1955.
[41] T. Nanba, M. Nishimura, Y. Miura, A theoretical interpretation of the chemical shift of 29Si NMR peaks in alkali borosilicate glasses, Geochmica et Cosmochimica Acta 68 (24) (2004) 5103–5111, doi:10.1016/j.gca.2004.05.042.
[42] C. Mendoza, S. Peuget, T. Charpentier, M. Moskura, R. Caraballo, O. Bouty, A.H. Mir, I. Monnet, C. Grygiel, C. Jégou, Oxide glass structure evolution under swift heavy ion irradiation, Nucl. Instrum. Methods Phys. Res., Sect. B 325 (2014) 54–65, doi:10.1016/j.nimb.2014.02.002.
[43] F. Angeli, O. Villain, S. Schuller, S. Ispas, T. Charpentier, Insight into sodium silicate glass structural organization by multinuclear NMR combined with first-principles calculations, Geochim. Cosmochim. Acta 75 (2011) 2453–2469.
[44] S. Peuget, T. Fares, E.A. Maugeri, R. Caraballo, T. Charpentier, L. Martel, J. Somers, A. Janssen, T. Wiss, F. Rozenblum, M. Magnin, X. Deschanels, C. Jégou, Effect of $^{10}b(n, \alpha)^7li$ irradiation on the structure of a sodium borosilicate glass, Nucl. Instrum. Methods Phys. Res., Sect. B 327 (2014) 22–28, doi:10.1016/j.nimb.2013.09.042.
[45] V.O. Glatter, O. Kratky, Small angle x-ray scattering., Acta Polymerica 36 (5) (1985), doi:10.1002/actp.1985.010360520.
[46] G. Kostorz, S.W. Lovesey, Neutron scattering - general introduction, in: G. Kostorz (Ed.), Neutron Scattering, Treatise on Materials Science & Technology, 15, Elsevier, 1979, pp. 1–67, doi:10.1016/B978-0-12-341815-9.50009-4.
[47] T.H. Elmer, M.E. Nordberg, G.B. Carrier, E.J. Korda, Phase separation in borosilicate glasses as seen by electron microscopy and scanning electron microscope, Journal of the American Ceramic Society 53 (4) (1970) 171–175.
[48] F. Angeli, O. Villain, S. Schuller, T. Charpentier, D. de Ligny, L. Bressel, L. Wondraczek, Effect of temperature and thermal history on borosilicate glass structure, Physical Review B 85 (054110) (2012).
[49] J. Wu, J. Stebbins, Quench rate and temperature effects on boron coordination in aluminoborosilicate melts, J. Non-Cryst. Solids (356) (2010).